Acta Pharmaceutica Sinica B 2025;15(1):494−507

Chinese Pharmaceutical Association
Institute of Materia Medica, Chinese Academy of Medical Sciences

Acta Pharmaceutica Sinica B

www.elsevier.com/locate/apsb
www.sciencedirect.com

ORIGINAL ARTICLE

"Relative symmetry with electronegativity of different key-groups" strategy for MRGPRX2 antagonist design and its effect on antigen-induced pulmonary inflammation

Jiayu Lu[a,†], Zhaomin Xia[a,†], Yongjing Zhang[a], He Wang[b], Wen Yang[a], Siqi Wang[a], Nan Wang[a], Yun Liu[c], Huaizhen He[a], Cheng Wang[a,*], Langchong He[a,*]

[a]*School of Pharmacy, Health Science Center, Xi'an Jiaotong University, Xi'an 710061, China*
[b]*Key Laboratory of Synthetic and Natural Functional Molecule Chemistry (Ministry of Education), College of Chemistry and Materials Science, Northwest University, Xi'an 710069, China*
[c]*Department of Respiratory and Critical Care Medicine, The Second Affiliated Hospital of Xi'an Jiaotong University, Xi'an 710004, China*

Received 28 October 2024; received in revised form 18 November 2024; accepted 28 November 2024

KEY WORDS

MRGPRX2;
Antagonist;
Diaryl urea;
Relative symmetry with electronegativity;
Antiallergic activity;
Antigen-induced pulmonary inflammation;
Structure−activity relationships;
Electrostatic

Abstract MRGPRX2 antagonists possess the potential for the treatment of allergic rhinitis, atopic dermatitis, and chronic urticaria. Previously, we identified a class of diaryl urea (DPU) MRGPRX2 antagonists with sub-micromolar IC_{50} values *in vitro*. However, the structure−activity relationship remains unclear. Herein, we adopted a "relative symmetry with electronegativity of different key-groups" strategy for further modification of DPUs to achieve a promising MRGPRX2 antagonist with higher activity and safety. Electrostatic potential energy analysis and biological evaluation revealed that B-1023 and B-5023, that possess relatively symmetric electron-withdrawing substituents, remarkable inhibited mast cell degranulation at a sub-micromolar IC_{50} *in vitro* and alleviated anaphylactic symptoms. Furthermore, B-1023, mitigated antigen-induced pulmonary inflammation (AIPI) in mice and competitively bonded to MRGPRX2. In summary, the "relative symmetry with electronegativity of different key-groups" strategy provided a drug design pattern for MRGPRX2 antagonists and identified promising anti-allergic precursors for AIPI treatment.

*Corresponding authors.
E-mail addresses: chengwang@mail.xjtu.edu.cn (Cheng Wang), helc@mail.xjtu.edu.cn (Langchong He).
[†]These authors made equal contributions to this work.
Peer review under the responsibility of Chinese Pharmaceutical Association and Institute of Materia Medica, Chinese Academy of Medical Sciences.

https://doi.org/10.1016/j.apsb.2024.11.023

complementarity

1. Introduction

Allergic diseases are prevalent with increasing incidence rates[1-4] and their unknown etiology and unpredictable onset significantly impair patient quality of life[5,6] and represent a growing public health concern. Mas-related G protein-coupled receptor X2 (MRGPRX2) on mast cells mediate IgE-independent allergic responses[7], that are associated with the development of various allergic disorders, such as allergic rhinitis[8], atopic dermatitis[9,10], and chronic urticaria[11]. Consequently, MRGPRX2 antagonists offer potential therapeutic avenues against these conditions[12,13].

Currently, no marketed drugs specifically target MRGPRX2, except EP262[14], which is currently undergoing clinical trials[15]. Other candidates remain in preclinical stages, some of which are derived from plant extracts such as phellodendrine[16], saikosaponin A (IC_{50} = 640.2 μmol/L)[17], isoliquiritigenin (IC_{50} = 50 μmol/L)[18], quercetin (IC_{50} = 100 μmol/L)[19], and imperatorin (IC_{50} = 50 μmol/L)[20]. However, high effective concentration and high cost for screening limit their therapeutic applicability. In contrast, small synthetic molecules allow for the efficient and rapid development of targeted antagonists through structural optimization. Synthetic compounds with significant MRGPRX2 inhibitory activity include dihydroquinazolinones: compound 1 (IC_{50} = 0.3 μmol/L), compound 2 (IC_{50} = 1.0 μmol/L)[21,22], phenalen-naphthalene compounds: GE1111 (IC_{50} = 4.7 μmol/L), GE0117 (IC_{50} = 20.77 μmol/L)[23,24], and diaryl ureas: DPU-17 (IC_{50} = 0.62 μmol/L), DPU-7 (IC_{50} = 0.79 μmol/L), DPU-16 (IC_{50} = 0.80 μmol/L)[25] (Fig. 1). Among these, we synthesized a class of diaryl ureas with promising activity in the context of antiallergic reactions mediated by MRGPRX2. As a representative compound, DPU-17 exhibited promising activity with IC_{50} values in the submicromolar range, thus necessitating further exploration of its structural basis for toxicity and activity to optimize efficacy and safety.

In this study, we proposed a "relative symmetry with electronegativity of different key-groups" strategy to further modifiy of DPUs for promising MRGPRX2 antagonists. Thirty compounds were synthesized by introducing various electron-withdrawing substituents onto the aromatic rings. Electrostatic potential energy analysis and biological evaluation revealed that B-1023 and B-5023, with relatively symmetric electron-withdrawing substituents, possessed improved activity and safety compared to that of DPU-17. Notably, B-1023 alleviated allergic reactions and mitigated antigen-induced pulmonary inflammation (AIPI) symptoms in mice, thus providing critical insights for developing potential antiallergic therapeutics.

2. Materials and methods

2.1. Reagents

Compound 48/80 (C48/80) was purchased from Sigma−Aldrich (C2313, St. Louis, MO, USA). *p*-Nitrophenyl *N*-acetyl-β-D-glucosamide was purchased from Macklin Biochemical Technology Co., Ltd. (CAS.3459-18-5, Shanghai, China). d_4-HA·2HCl (A, A, B, B-D_4, 98%) was purchased from Cambridge Isotope Laboratories, Inc. (No.DLM-2299-PK, Tewksbury, MA, USA). Fluo-3, AM ester, and Pluronic F-127 were purchased from Biotium, Inc. (Cat# 50010; Cat#: 59000; Fremont, CA, USA). HPLC-grade methanol and acetonitrile were purchased from Fisher Scientific (Waltham, MA, USA). The IL-8 ELISA Kit was purchased from Sino Biological, Inc. (Cat: KIT10098; Beijing, China). Tyrode's solution (TM buffer: NaCl 119 mmol/L, KCl 4.7 mmol/L, $CaCl_2$ 2.5 mmol/L, $MgSO_4$ 1.1 mmol/L, KH_2PO_4 1.1 mmol/L, HEPES 10 mmol/L, glucose 5 mmol/L, and BSA 6.3 mmol/L, pH = 7) and calcium imaging buffer (CIB: NaCl 125 mmol/L, KCl 3 mmol/L, $CaCl_2$ 2.5 mmol/L, $MgCl_2$ 0.6 mmol/L, HEPES 10 mmol/L, glucose 20 mmol/L, $NaHCO_3$ 1.2 mmol/L, and sucrose 20 mmol/L, pH = 7.4) were prepared separately before the experiments. All synthetic ingredients were purchased from Macklin Biochemical Technology Co., Ltd. (Shanghai, China).

2.2. Synthesis procedure of all compounds

2.2.1. Procedures for the synthesis of series A

The general synthetic procedure for A-series compounds was similar to that reported previously[25].

2.2.2. Procedures for the synthesis of series B

To the BTC solution (4 mmol, 0.4 equiv.) in dry THF (15 mL), one substituted aniline (10 mmol, 1.0 equiv.) dissolved in dry THF (20 mL) was slowly dropped through a pressure-equalizing dropping funnel at RT. Subsequently, Et_3N (12 mmol, 1.2 equiv.) dissolved in dry THF (15 mL) was slowly added dropwise and stirred for 5 min. The organic solvent was then evaporated, and aniline (10 mmol, 1.0 equiv.) in dry THF (20 mL) was slowly dripped into the residue. The mixture was stirred at 45 °C for 3−6 h. The solvent was then removed under reduced pressure, and the crude material was dissolved in dichloromethane (DCM) (20 mL) and washed with water (3 × 20 mL). The organic phase was dried over sodium sulfate (Na_2SO_4), filtered, and concentrated under reduced pressure to obtain the crude product that was then separated and purified using chromatography to obtain B-1023 to B-5023. B-10023 is a by-product of the synthesis of B-2023.

At 0 °C under the protection of nitrogen (N_2), *N*,*N*-diisopropyl ethylamine (DIPEA) (12 mmol, 4.0 equiv.) was dropped into a solution of 4-aminobenzenesulfonic acid (3 mmol, 1.0 equiv.) in dry *N*,*N*-dimethylformamide (DMF) (10 mL), and the mixture was stirred for 5 min. Subsequently, 1-isocyanato-4-(trifluoromethyl) benzene (3 mmol, 1.0 equiv.) dissolved in dry DMF (10 mL) was added dropwise. The mixture was allowed to reach room temperature (RT) and was stirred for 6 h. After the completion of the reaction, the solvent was removed under reduced pressure to obtain the residue which then separated and purified by chromatography to obtain B-6023.

To a solution of 1-isocyanato-4-(trifluoromethyl) benzene (10 mmol, 1.0 equiv.) in dry THF (15 mL) was added to the substituted aniline (10 mmol) in dry THF (15 mL) at 0 °C, and the mixture was stirred for 3−6 h at RT. A precipitate was produced during the reaction and filtered after completion of the reaction.

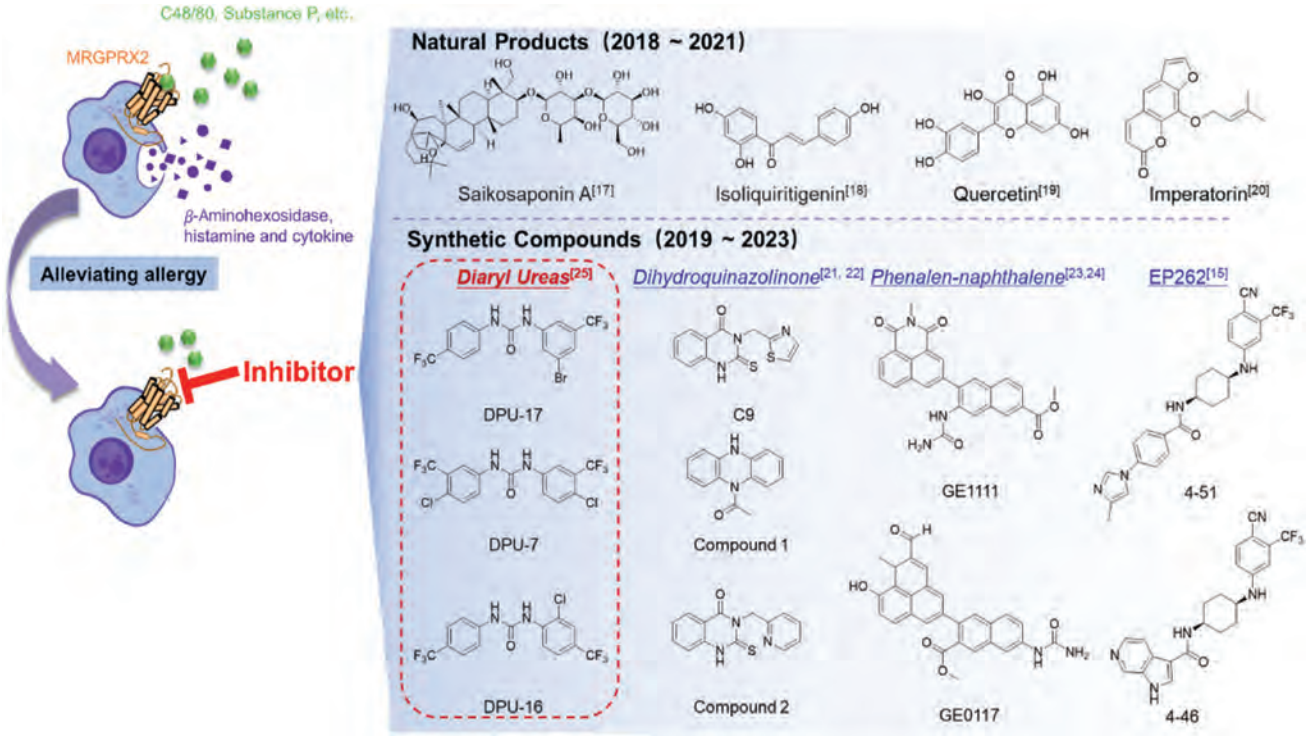

Figure 1 Compounds with inhibition of MRGPRX2 activity have been reported.

The filter cake was washed with THF (3 × 15 mL) and separated using a chromatographic column to obtain pure B-7023 to B-9023 and B-17023. B-11023 was a commercially purchased compound.

Iron powder (25 mmol, 5.0 equiv.) and ammonium chloride (NH_4Cl) (2.5 mmol, 0.5 equiv.) in water (15 mL) were added to the solution of B-1023 to B-4023 (5 mmol, 1.0 equiv.) in ethyl alcohol (EtOH) (30 mL) at 50−55 °C, and the mixture was refluxed for 1−3 h. After the completion of the reaction, the mixture was filtered, and the filtrate was concentrated under reduced pressure. The residue was dissolved in water (10 mL) and adjusted to a pH of 7−8 using a saturated sodium bicarbonate ($NaHCO_3$) solution. It was then extracted with ethyl acetate (EA) (3 × 20 mL). The organic phase was then dried over anhydrous Na_2SO_4 and concentrated under reduced pressure. The residue was then subjected to chromatography to obtain pure B-12023 to B-15023.

Hydrogen peroxide (H_2O_2) (0.12 mL) (30%) and potassium carbonate (K_2CO_3) (1.5 mmol, 1.5 equiv.) were added to the solution of B-5023 (1 mmol, 1.0 equiv.) dissolved in dimethyl sulfoxide (DMSO) (0.3 mL) at 0 °C. The mixture was stirred for 5 min at RT, and distilled water (5 mL) was slowly added. The resulting mixture was cooled and filtered to obtain B-16023.

The first step of B-18023 synthesis was similar to that of B-7023 to B-9023 and B-17023. To a solution of 1-isocyanato-4-(trifluoromethyl) benzene in dry THF was added the 3-nitro-5-(trifluoromethyl) aniline in dry THF at 0 °C. Then, the solution was heated for 12h at 45 °C. The second step of B-18023 synthesis was similar to that of B-12023 to B-15023. The mixture was heated to 53 °C for 3 h, and the residue was chromatographed to obtain pure B-18023.

2.2.3. *Procedures for the synthesis of series C*

DIPEA (1.2 mmol, 1.2 equiv.) was slowly added to the solution of substituted carboxylic acid (1.1 mmol, 1.1 equiv.) and *O*-(7-azabenzotriazol-1-yl)-*N*,*N*,*N*′,*N*′-tetramethyluronium hexafluorophosphate (HATU) (1.1 mmol, 1.1 equiv.) in dry DMF (10 mL) at 0 °C, and the solution was stirred for 15 min at 0 °C. Then, B-12023/B-15023 (1 mmol, 1.0 equiv.) dissolved in dry DMF (5 mL) was added, and the solution was stirred for 3−12 h at RT. After the completion of the reaction, the mixture was extracted with EA (3 × 15 mL) and water (3 × 150 mL). The organic phase was dried over Na_2SO_4, filtered, and then concentrated under reduced pressure. The residue was separated and purified using a chromatography column to obtain C-1023 to C-6023.

All compounds were characterized by ^{1}H NMR and ^{13}C NMR (Bruker AVANCE 400 MHZ spectrometer) and HRMS (WATERS I-Class VION IMS QTOF). The purity was determined by HPLC at > 95% on the SHIMADZU LC-2030C system. The compound characterization was listed in the Supporting Information file.

2.3. *Cell lines and animals*

Human Laboratory of Allergic Disease 2 Mast Cells (LAD2 cells) provided by Dr. A. Kirshenbaum and Dr. D. Metcalfe (NIH, Bethesda, MD, USA) were maintained in StemPro-34 medium supplemented with 10 mL/L of StemPro nutrient supplement, 1:100 penicillin−streptomycin, 2 mmol/L L-glutamine, and 100 ng/mL of human stem cell factor at 37 °C under 5% CO_2. MRGPRX2-overexpressing HEK293 (MRGPRX2-HEK293) cells were cultured in Dulbecco's modified Eagle's medium containing 10% fetal bovine serum, 100 U/mL penicillin/streptomycin, and 0.5 μg/mL puromycin at 37 °C under 5% CO_2.

This study was conducted in accordance with the Guide for the Care and Use of Laboratory Animals of the National Institutes of Health. The experimental protocols for mice were approved by the Animal Ethics Committee of Xi'an Jiaotong University, Xi'an, China (Permit Number: XJTU 2019−714). ICR mice weighing

18−22 g were obtained from the Laboratory Animal Center of Xi'an Jiaotong University (Xi'an, China) and provided with food and water optionally. All experiments requiring identical administration to the animals were performed by investigators who were blinded to the experimental conditions.

2.4. Detection of cell viability

A total of 1×10^5 LAD2 cells in the logarithmic growth phase were uniformly seeded into 96-well plates for the treated and control groups. The blank group was seeded with culture medium. With the medium as the solvent, 10 μL of the compound was added to each well of the treated group, and 10 μL of the medium was added to the control and the blank groups, respectively. The cells were then incubated for 24 h. Then, 10 μL of CCK-8 reagent was added, and the plate was incubated for 1.5 h. The optical density (OD) of each well was measured at 450 nm, and LAD2 cell viability was calculated as in Eq. (1):

$$\text{Cell viability}\ (\%) = \frac{\text{OD}_{\text{Treated}} - \text{OD}_{\text{Blank}}}{\text{OD}_{\text{Control}} - \text{OD}_{\text{Blank}}} \times 100 \quad (1)$$

2.5. Detection of β-hexosaminidase release

The logarithmic phase well-conditioned LAD2 cells (1×10^6) were uniformly seeded into 96-well plates and cultured for 2 h in an incubator. After centrifuging at 400×*g* for 5 min, the supernatant was discarded, and 50 μL of TM buffer with final concentrations of different compounds was added to each well of the treated group. The control group was incubated with the TM buffer for 30 min. Next, 50 μL of C48/80 at 60 μg/mL was added, and the incubation continued for another 30 min. After incubation, the cells were centrifuged, and the supernatant was collected. Next, 0.1% Triton X-100 lysate was added to the control group to lyse the cells that were then centrifuged to obtain the lysis supernatant. Then, 50 μL of *p*-nitrophenyl *N*-acetyl-β-D-glucosamide in 0.1 mol/L citric acid/sodium citrate buffer was added to the supernatants, and the plate was incubated for 2 h at 37 °C. The stop buffer (0.1 mol/L Na_2CO_3 and 0.1 mol/L $NaHCO_3$ [9:1]) was added, and the plate was measured at 405 nm using a microplate reader. The percentage of β-hexosaminidase that was released was calculated as in Eq. (2):

$$\text{Percentage of } \beta\text{-hexosaminidase } (\%) = \text{The absorbance of the culture supernatant/absorbance of the total cell lysate supernatant} \times 100 \quad (2)$$

2.6. Detection of histamine release in vitro

The treatment for histamine release was similar to that used in the β-hexosaminidase assay. C48/80 was used as an agonist. After incubation with the compounds, 50 μL of supernatant was collected, and 100 μL of d_4-HA in acetonitrile (ACN) was then added. Histamine levels were evaluated using HPLC−MS as previously described[26].

2.7. Detection of IL-8 release

The medium containing 30 μg/mL C48/80 and compounds (1, 5, and 10 μmol/L) was added to LAD2 cells (1×10^6/well), and the cells were incubated for 6 h. For the control group, the cells were treated with a medium only. The release of IL-8 was detected using an ELISA kit-based method.

2.8. Paw swell and extravasation in mice

Adult mice were randomly divided into treatment (1, 5, or 10 mg/kg), C48/80, and control groups. The compounds were diluted in DMSO-C_2H_5OH-PEG400-H_2O (1:9:50:40) to concentrations of 0.1, 0.5, and 1 mg/mL, and 200 μL was administered by gavage to every mouse in the treated and C48/80 groups. Two hours later, mice were anesthetized and intravenously injected with 200 μL of 0.4% Evans blue in saline. The thicknesses of the left and right paws (La and Ra, respectively) were measured. Next, 5 μL of saline and 60 μg/mL of C48/80 were injected into the left and right paws, respectively. Fifteen minutes later, paw thickness was again measured, and the mice were sacrificed by cervical dislocation. The paws were clipped and dried for 24 h at 60 °C and then weighed. Then, 450 μL of acetone-saline (7:3) mixture was added to the paw tissue. Paw tissue was cut, sonicated, and centrifuged to obtain the supernatant. The OD of each well was measured at a wavelength of 620 nm.

2.9. Detection of serum histamine release in vivo

The experimental grouping and gavage methods were consistent with the detection of paw swelling and Evans blue extravasation in mice. 2 h later, mice were intravenously injected with 200 μL of 100 μg/mL C48/80 in saline. Retro-orbital blood was collected 1 h after administration, placed in EP tubes, and stored on ice. The collected blood was centrifuged for 20 min at 14,000×*g* at 4 °C to obtain the serum. A 50 μL aliquot of serum was transferred into a clean EP tube, and 50 ng/mL d_4-HA (serum: d_4-HA = 1:2, *v*/*v*) was added. Next, the mixture was centrifuged for 20 min at 14,000×*g* at 4 °C, and the supernatants were analyzed according to a previously reported procedure[26] by HPLC−MS.

2.10. Skin toluidine blue staining in mice

Adult mice were randomly divided into treatment (10 mg/kg), C48/80, and control groups. The drug was administered in the same manner as it was for the paw swelling and extravasation assays. Then, mice were anesthetized, and 5 μL saline or 100 μg/mL C48/80 was injected into the left or right paw. After 15 min, the mice were sacrificed, and the skin tissue of the paw was cut and fixed in 4% paraformaldehyde. Skin tissue was embedded, sectioned, deparaffinized, antigen-repaired, and blocked. The skin tissue was stained with toluidine blue, sealed, and imaged using an ECLIPSE Ci-L imaging microscope (Nikon, Tokyo, Japan).

2.11. Detection of the body temperature of mice

Adult mice were grouped and treated in a manner consistent with the skin toluidine blue staining. Subsequently, the initial body temperature of the mice was recorded. Then, mice were intravenously injected with 200 μL of 100 μg/mL C48/80 in saline, and the body temperature was recorded every 5 min for 30 min using a digital thermometer (BL-410 Biofunction system).

2.12. Antigen-induced pulmonary inflammation (AIPI) and therapeutic effective evaluation

OVA was used as the antigen to induce pulmonary inflammation in mice. Briefly, female C57BL/6 mice (six-to eight-week-old) were intraperitoneally sensitized by 0.25 mg/kg OVA on Days 1, 3, 5, and 7. On Days 21, 23, 25, 27, and 29, mice were challenged with 1% atomized OVA in a sealed container for 30 min. Thirty minutes before each challenge, B-0123 was orally administered. The mice in the vehicle group inhaled atomized PBS. After the final challenge, mice were subjected to AHR testing, and bronchoalveolar lavage was collected within 24 h. AHR was detected using a Flexivent (Canada) after methacholine challenge. RN, Rrs, G, and Cr levels were recorded. The BALF was collected and centrifuged to separate the supernatant and lymphocytes. Th2 cytokines in the lavage fluid were detected using ELISA. Wright & Giemsa staining was used for lymphocyte counting. Serum IgE was also measured by ELISA. Hematoxylin and eosin (HE), MASSON, and PAS staining were performed on lung sections.

2.13. Electronegativity and molecular surface electrostatic potential prediction

The electronegativity and molecular surface electrostatic potential of the compounds both were evaluated using Density Functional Theory (DFT). The geometries and energies of all complexes were computed at the B3LYP-D3 functional and def2-SVP basis level of theory using the program Gaussian 16 (Gaussian, Inc.).

2.14. Intracellular Ca^{2+} mobilization assay

All of the compounds were dissolved to the required concentrations in CIB. The incubation buffer consisted of 1 μL Fluo-3, 3 μL Pluronic F-127, and 996 μL CIB. Logarithmic phase well-conditioned MRGPRX2-HEK293 cells were seeded into 96-well plates at 1×10^4 cells per well and incubated for 12 h. The next day, the medium was discarded, and the cells were washed twice with CIB. Then, the compounds in the incubation buffer at concentrations of 1, 5, and 10 μmol/L were added to the treated group. An incubation buffer was added to the control group, and all groups were incubated for 30 min. After removing the liquid, the plate was washed twice with CIB, and 50 μL of CIB was added. A fluorescent microscope (Nikon) was used to record calcium mobilization after 50 μL of C48/80 (60 μg/mL) was added.

2.15. Competitive binding assay of compounds with fluorescent probes targeting MRGPRX2

MRGPRX2-HEK293 cells were seeded into 96-well plates at a density of 1×10^5 cells/well and incubated for 24 h. The Fluorescent Probe for MRGPRX2, ZX2, was diluted with HBSS to 2 μmol/L, and compounds were prepared at the required concentrations in the ZX2 solution. The mixture was added to each well and incubated at 37 °C in the dark for 40 min. After incubation, the supernatant was discarded, and 100 μL of HBSS buffer was added to each well. The plates were analyzed using a microplate reader. The fluorescence intensity of the cells was measured at excitation and emission wavelengths of 435 and 483 nm, respectively, and the bottom-reading mode was selected. The images were captured using a fluorescence microscope (Nikon).

2.16. Cell membrane chromatography

For measuring the K_D value, the relative standard method was used as described by Ma et al[27]. Under the same analytical conditions, the retention of the analyte and reference on the CMC column was investigated and the K_D value of the analyte was calculated according to the K_D value of the reference. The formula is shown in Eq. (3):

$$K_{D_x} = \frac{k_s}{k_x} \cdot K_{D_s} \tag{3}$$

where k_s is the reference retention factor, k_x is the analyte retention factor, K_{Ds} is the dissociation constant of the reference, and K_{Dx} can be obtained. The K_{Ds} values of reference (*R*)-ZINC-3573 were obtained from a reported article[28]. The competitive binding study was performed as described previously[29]. (*R*)-ZINC-3573 at different concentrations was added to ultrapure water as the mobile phase, and the retention of the substance to be measured was recorded.

2.17. Molecular docking

All compound structures were drawn using ChemDraw 21.0.0 (PerkinElmer Inc.) and transformed into MOL2 format using Chem3D 8.0 (PerkinElmer Inc.). Then, these compounds were depicted and optimized by Powell's method with Tripos force field with convergence criterion at 0.05 kcal/(Å mol) and assigned with the Gasteiger−Hückel method by SYBYL-X 2.0. The MRGPRX2 model was downloaded from PDB.BANK (PDB code: 7S8N) and then optimized by SYBYL-X 2.0 to extract the ligand, remove the redundant amino acid residue, and add hydrogen. The binding model of MRGPRX2 and the compounds were determined using the Surflex-Dock (SFXC) mode, and PyMOL (https://pymol.org/2/) was used to visualize the docking results. CoMFA analysis was carried in SYBYL-X 2.0 following the protocol in the previous literature[30].

2.18. Statistical analysis

The data are presented as mean ± SD. One-way analysis of variance (ANOVA) was performed using GraphPad Prism 10.1.2 (GraphPad Software).

3. Results and discussion

3.1. Design and synthesis

Series A: DPU-17 exhibited favorable activity with an IC_{50} of 0.62 ± 0.09 μmol/L; however, it significantly affected the viability of LAD2 cells. To determine the effect of group location on the activity and toxicity of DPU-17, six compounds from Series A were designed by removing one, two, or three substituents from DPU-17.

As presented in Scheme 1, the compounds in Series A were synthesized by reacting the substituted aniline with bis(trichloromethyl) carbonate (BTC) in the presence of triethylamine (Et_3N)[25].

Series B: To further tune the reactivity and toxicity of Series A, 18 compounds were synthesized by introducing various electron-withdrawing and electron-donating groups. B-1023 to B-5023

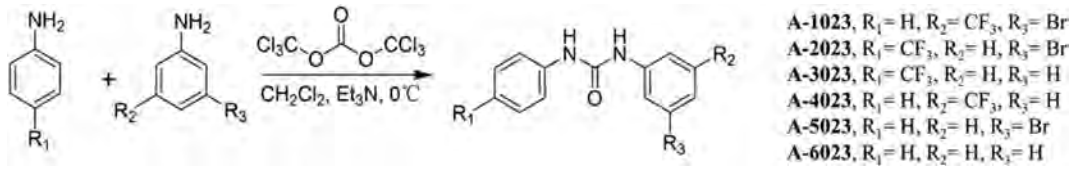

Scheme 1 Synthesis of series A.

were synthesized using a method similar to that used for Series A. The reaction of 1-isocyanato-4-(trifluoromethyl) benzene and substituted aniline gave B-6023 to B-9023 and B-17023. After reacting 1-isocyanato-4-(trifluoromethyl) benzene with 3-bromo-5-nitroaniline, NO_2 is reduced to NH_2 to obtain B-18023.The reduction of nitro groups of B-1023 to B-4023 yielded B-12023 to B-15023, and the hydrolysis of the cyano of B-5023 resulted in B-16023 (Scheme 2).

Series C: To further improve the structural diversity of diaryl ureas, we introduced several frequently occurring nitrogen heterocycles in FDA-approved drugs[31]. The amino groups of B-12023 and B-15023 were dehydrated and condensed to form amides with the carboxyl groups of 5-(trifluoromethyl)-1*H*-pyrazole-4-carboxylic acid, 4-acetamidobenzoic acid and 1H-pyrrolo [2,3-*b*] pyridine-3-carboxylic acid, respectively, thus yielding six compounds in Series C (Scheme 3).

3.2. Preliminary investigation of the toxicity and antiallergic activity of newly designed compounds

Mast cells are primary effectors in allergic reactions by secreting *β*-hexosaminidase, histamine and various inflammatory and immunomodulatory substances[7]. Therefore, laboratory of allergic diseases 2 (LAD2) cells, which most closely resemble mature human mast cells[32], were used to evaluate the antiallergic activity of candidate compounds. The effects of compounds from series A on viability and *β*-hexosaminidase release of LAD2 cells were initially evaluated (Fig. 2A). A-6023 possessing a diaryl urea parent structure exhibited both antiallergic activity toxic and cytotoxicity on LAD2 cells at 10 μmol/L. A-3023 and A-4023 exhibited attenuated cytotoxicity, indicating that mono-substituted CF_3 reduces toxicity. A-3023 was much more potent than A-4023, thus indicating that CF_3 at the para-position is

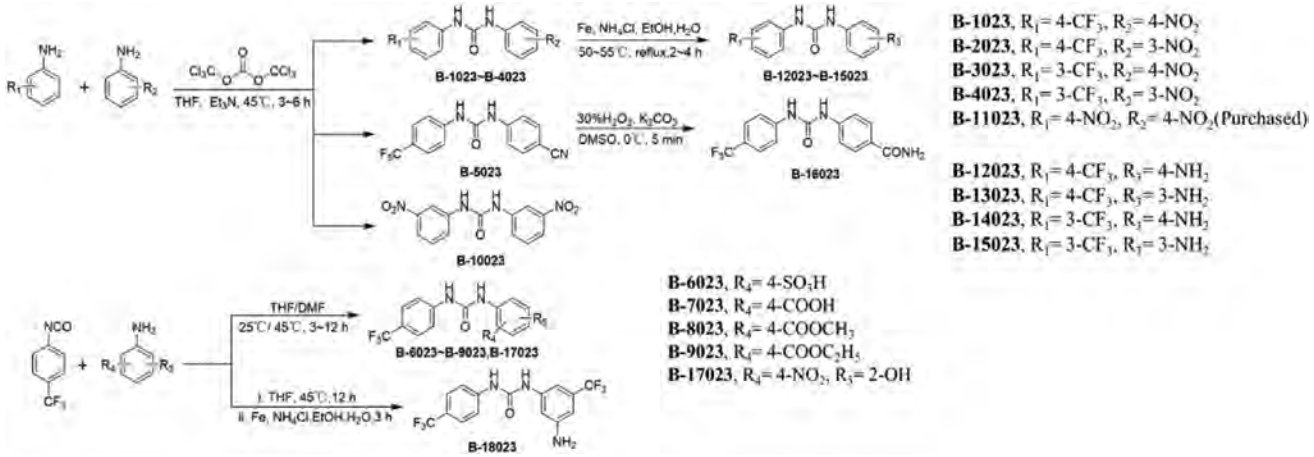

Scheme 2 Synthesis of series B.

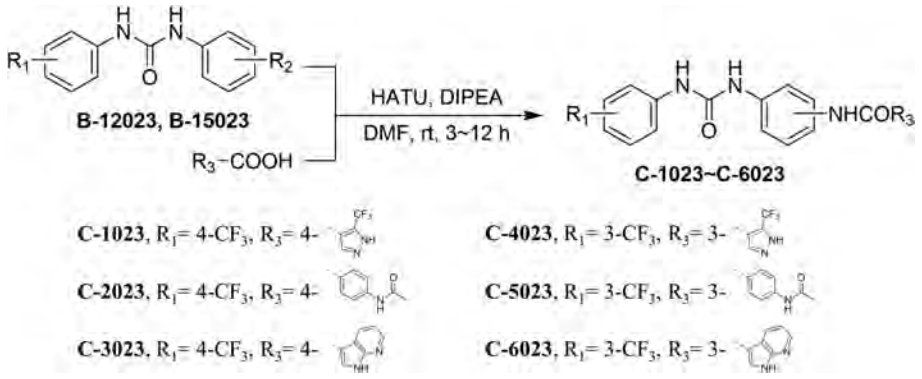

Scheme 3 Synthesis of series C.

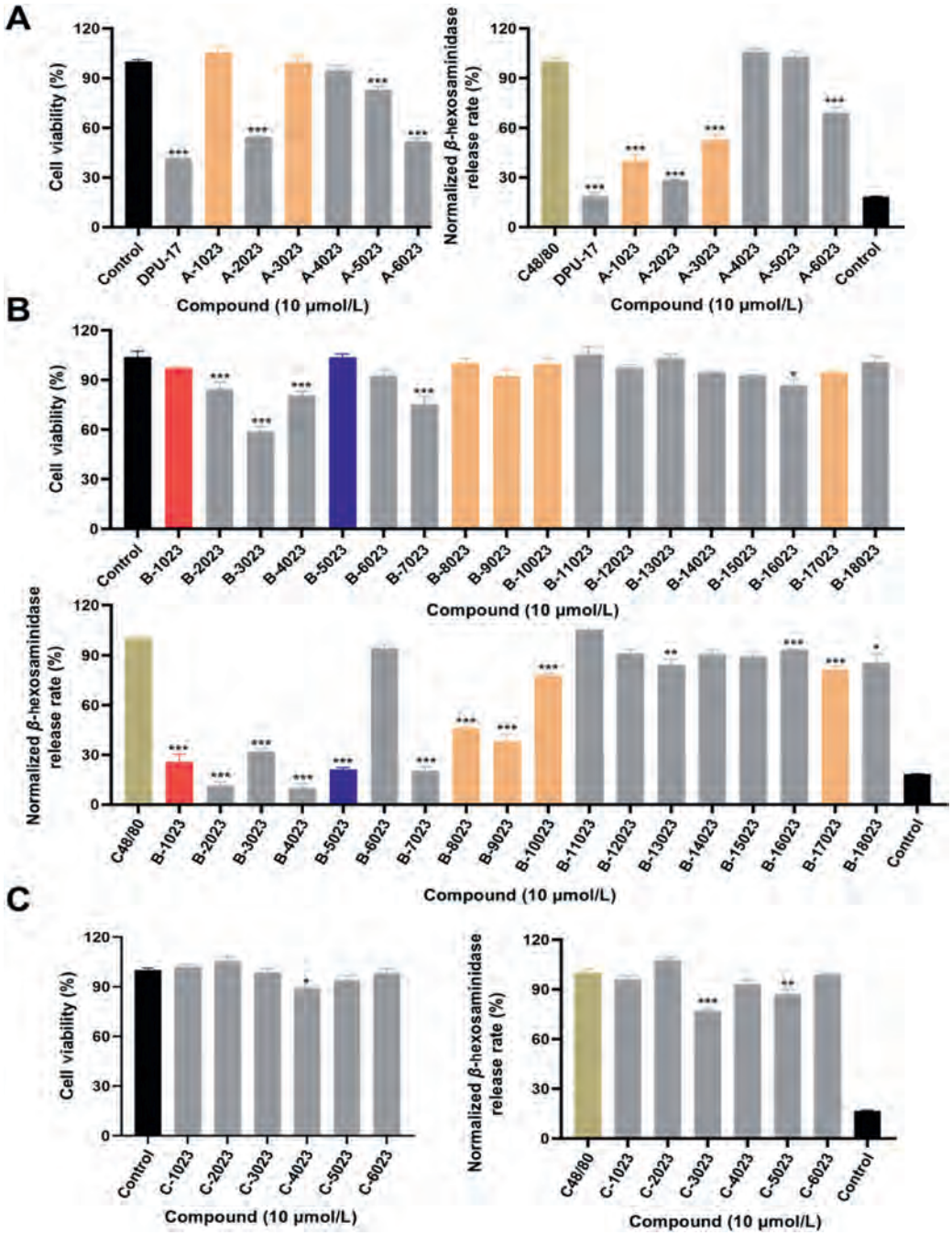

Figure 2 Evaluation of the cytotoxicity and β-hexosidosidase release of the A, B and C series compounds. The cytotoxicity and β-hexosidosidase release inhibition on LAD2 cells at 10 μmol/L of series A(A), B(B) and C(C). Data are presented as mean ± SD ($n = 3$), $^{***}P < 0.001$ and $^{*}P < 0.05$ *vs.* Control in cytotoxicity evaluation; $^{***}P < 0.001$, $^{**}P < 0.01$ and $^{*}P < 0.05$ *vs.* C48/80 group.

critical for maintaining antiallergic activity. Mono-substitution with bromine (A-5023) resulted in no antiallergic activity or cytotoxicity. Compared to that of A-1023, A-2023 exhibited much higher toxicity, thus indicating that the substitution positions of CF_3 also play a critical role in cytotoxicity. Therefore, in the subsequent structural design, CF_3 will be kept on one side of the para-position or meta-position to reduce toxicity and maintain activity. Further, according to the negatively charged active pocket in MRGPRX2[33], electron-withdrawing substituents, such as NO_2, SO_3H, COOH, $COOCH_3$, and nitrogen heterocycles frequently occurring in FDA-approved drugs were introduced into the phenyl ring in Series B and C, respectively. As presented in Fig. 2B, compared to B-2023 to B-4023, B-1023 was nontoxic with NO_2 and CF_3 at the para-position. This indicates that retaining electron-withdrawing substituents in the para-position is more favorable for reducing toxicity. Similarly, the remaining compounds with electron-withdrawing substituents at the para position were non-cytotoxic, with the exceptions of B-7023, B-16023 and C-4023.

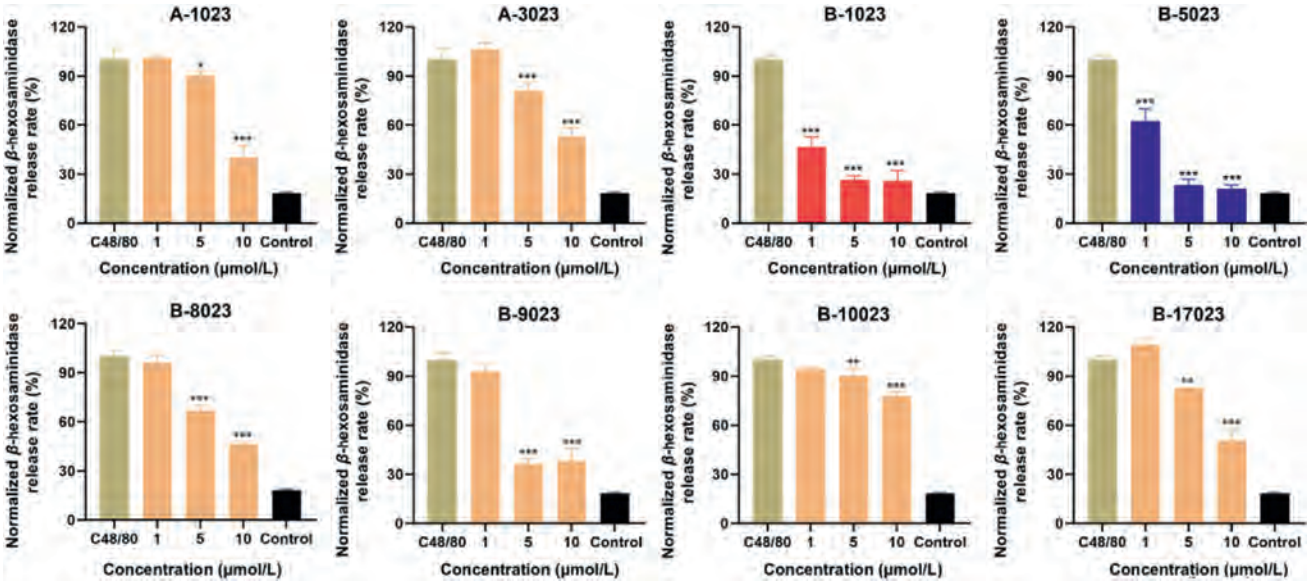

Figure 3 The non-cytotoxic and active compounds inhibited β-hexosidosidase release induced by C48/80 at 1, 5 and 10 μmol/L. Data are presented as mean ± SD ($n = 3$), ***$P < 0.001$, **$P < 0.01$ and *$P < 0.05$ *vs.* C48/80.

In regard to antiallergic activity, introducing electron-withdrawing substituents increased the antiallergic potency (B-1023 to B-4023), whereas introducing electron-donating substituents decreased the antiallergic potency (B-12023 to B-15023). We then replaced the nitro group in B-1023 with a cyano group(B-5023), carboxyl group (B-7023), and ester group (B-8023 and B-9023), and the electronegativity of the introduced groups was in order from largest to smallest. These results suggested that compounds with stronger electron-withdrawing groups possessed more potent antiallergic activities. The inactivity of B-6023 may be due to the large size of its sulfonate group, which is unable to bind to the MRGPRX2 cavity due to site-blocking effects. Moreover, by comparing B-1023 to B-10023, and B-4023 to B-11023, we reconfirmed that CF_3 plays a crucial role in antiallergic activity. Additionally, Series C exhibited no obvious antiallergic activity (Fig. 2C). Molecular docking suggested that the large size of the substituents resulted in an inability to reach the binding pocket of MRGPRX2 (Supporting Information Fig. S1). In a word, comparing the compounds in series A, B and C, the majority of compounds in series A and B have better antiallergic activity than compounds in series C. Through comparing the size and electron-withdrawing capability of substitutes, we found that compounds in series A and B have smaller and stronger electron-withdrawing substituents substitute of benzene, which is guidance for modification of DPUs.

Subsequently, 12 non-toxic and the most effective compounds were examined for their antiallergic activity at 1, 5, and 10 μmol/L (Fig. 3 and Supporting Information Fig. S2), they were all able to inhibit the release of β-hexosaminidase to varying degrees. B-1023 and B-5023 exhibited the most potential antiallergic ability.

3.3. Introduction of electron-withdrawing substituents enhances electronegativity to improve the antiallergic activity of DPUs

To further validate the relevance of electron-withdrawing substituents on diaryl ureas to their antiallergic activity, a portion of

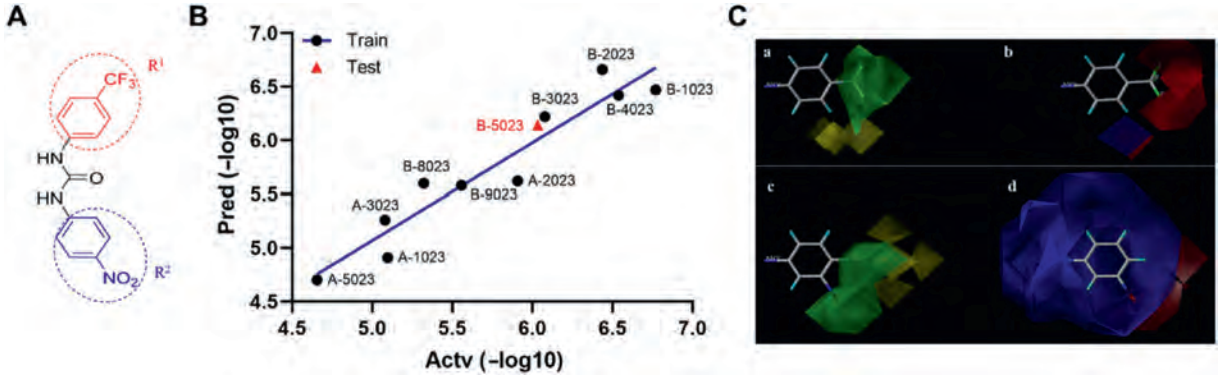

Figure 4 The structure−activity relationship results by Topomer CoMFA. (A) The counting model for CoMFA study; (B) Experimental and calculated pIC_{50} for the CoMFA analysis of the training set and test set; (C) The contour map based on template compound B-2023; a and c for R^1; b and d for R^2.

Table 1 Experimental and predicted pIC_{50} for Topomer CoMFA.

Compound	Experimental pIC_{50}	Pre pIC_{50}
Training set		
A-1023	5.10	4.91
A-2023	5.91	5.62
A-3023	5.08	5.26
A-5023	4.66	4.7
B-1023	6.77	6.47
B-2023	6.44	6.66
B-3023	6.08	6.22
B-4023	6.54	6.42
B-8023	5.32	5.6
B-9023	5.56	5.58
Test set		
B-5023	6.03	6.14

the active compounds was subjected to structure−activity relationship analysis using Topomer CoMFA. The most active 10 compounds were used as the template, and all compounds were fragmented into three parts that included R^1 (red), R^2 (blue) and a common skeleton (black) by automatic segmentation as shown in Fig. 4A. The experimental and predicted pIC_{50} values obtained using Topomer CoMFA are presented in Table 1 and plotted in Fig. 4B. The high q^2 (0.561) and r^2 (0.911) values indicated the high predictive ability and reliability of the model. As presented in Fig. 4C a and c, the sterically favored regions in B-2023 were in proximity to the meta- and para-positions of the phenyl ring (green contours), thus indicating that compounds with larger substitutions are essential for high anti-pseudo-allergic activity. Moreover, negatively charged favorable red regions were observed at the meta- and para-positions of the phenyl group in A-1023 (Fig. 4C b and d), which attributed to the bromo-substitution at the meta-position of the phenyl group. That indicated that an electron-

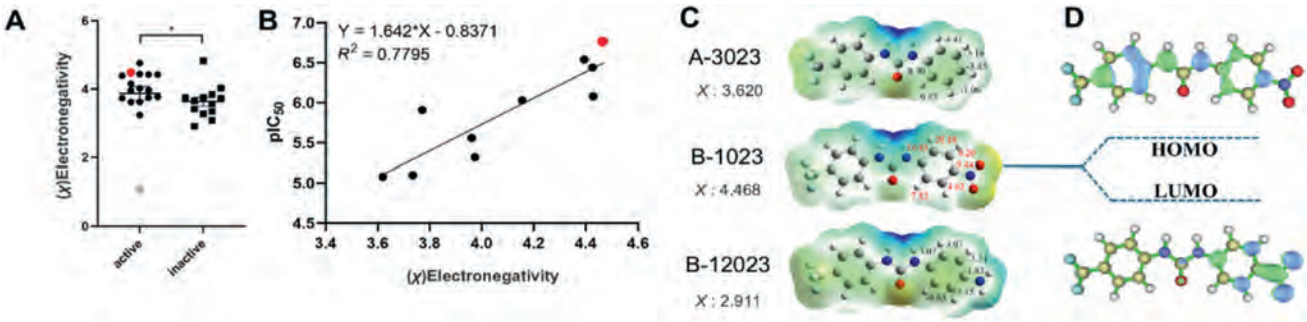

Figure 5 Activity and electronegativity correlation analysis. (A) The electronegativity distribution of active and inactive classes in 10 μmol/L; B-7023, the grey point, was not counted and B-1023 was hightlighted in red; $*P < 0.05$ with t test. (B) Correlation curve between pIC_{50} and electronegativity of 11 active compounds; B-1023 was hightlighted in red; (C) Electrostatic potential energy distribution on the surface of A-3023, B-1023 and B-12023; The maximum electrostatic potential energy of the carbon atom on the benzene ring is labelled; (D) Electron cloud distribution of the HOMO and LUMO orbitals of B-1023.

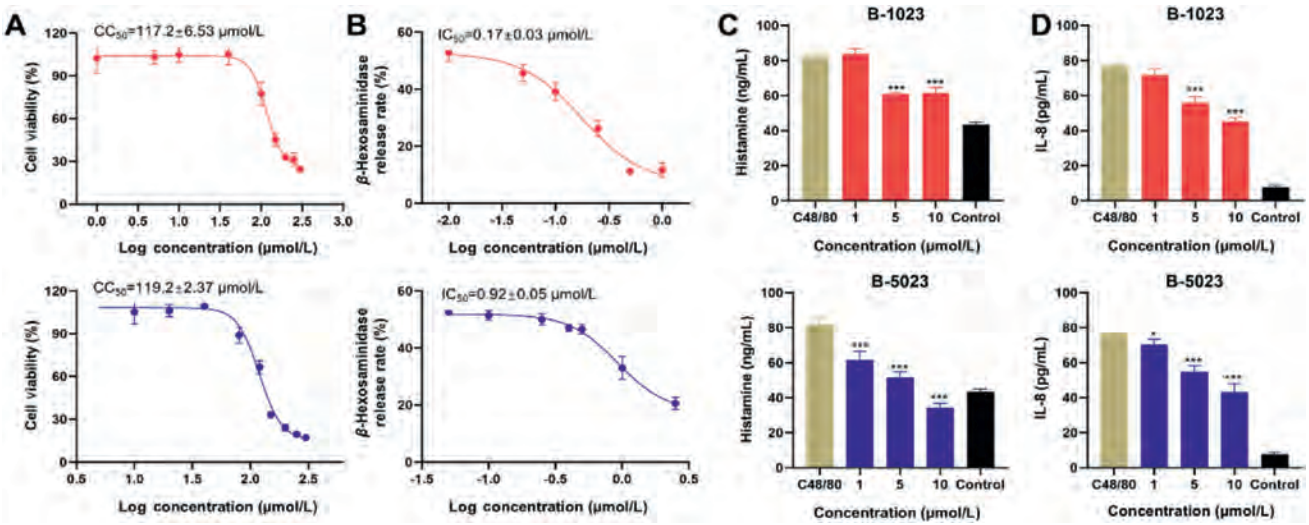

Figure 6 B-1023 and B-5023 inhibited LAD2 cell degranulation induced by C48/80. (A) The concentration of cytotoxicity 50% (CC_{50}) of B-1023 and B-5023; (B) The IC_{50} of B-1023 and B-5023 inhibited the β-hexosidosidase release induced by C48/80 in LAD2 cells; (C) The histamine release inhibited by B-1023 and B-5023 in 1, 5, 10 μmol/L compared with C48/80 group; (D) The IL-8 release inhibited by B-1023 and B-5023 in 1, 5, 10 μmol/L compared with C48/80 group. Data are presented as mean ± SD ($n = 3$), $***P < 0.001$ and $*P < 0.05$ *vs.* C48/80.

withdrawing substituent enhanced activity and this supports the observation that compounds B-1023, B-2023, and B-3023 exhibited highly beneficial effects.

To further investigate the effect of substituent electronegativity on the activity of compounds, we have conducted a comprehensive analysis of the electronegativity-activity relationship, with the exception of B-7023 due to its excessively low χ value. Compounds exhibiting antiallergic activity exhibited higher electronegativity than did those without activity (Fig. 5A and Supporting Information Table S1). Ten compounds with IC_{50} values of less than 10 μmol/L in the preliminary screening were selected for the correlation analysis between pIC_{50} and electronegativity. The R^2 value of the correlation was 0.7795 (Fig. 5B), indicating that compounds with better electronegativity possessed stronger activity. An in-depth analysis of the surface electrostatic potential energy distribution of the most active compound, B-1023 (Fig. 5C) revealed that the benzene ring region to which NO_2 is attached exhibited a large electrostatic potential value. The electrostatic potential decreased when NO_2 was replaced with H (A-3023) or NH_2(B-12023). This indicates that this region of B-1023 is more accessible to electrons and more electrophilic. Therefore, B-1023 is more likely to bind to the negatively charged pocket of MRGPRX2. Molecular docking also revealed that the NO_2 side of B-1023 extends deeply into the cavity, whereas the NH_2 side of B-12023 is outside the cavity. Further analysis of the electron-leaping orbitals of B-1023 (Fig. 5D) indicated that the LUMO of the nitro-substituted benzene ring possessed a large electron cloud density with a tendency to bond and a higher likelihood of mutual attraction with the protein. This observation underscores the rationality of the design strategy based on the complementary electrostatic effect.

3.4. B-1023 and B-5023 exhibited the strongest antiallergic activity

Among all the compounds evaluated, B-1023 and B-5023 demonstrated the most significant antiallergic activity and safety,

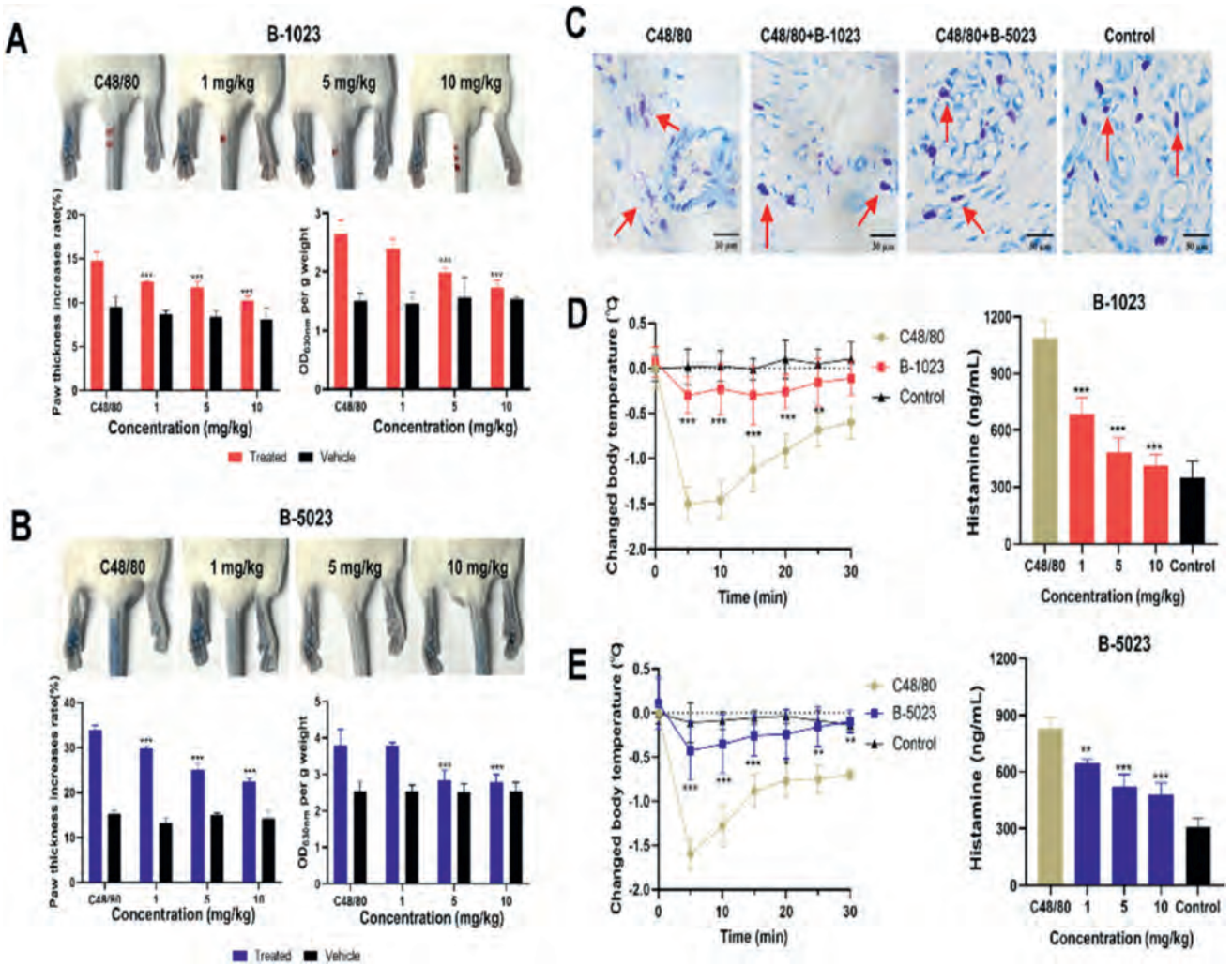

Figure 7 B-1023 and B-5023 inhibited C48/80-induced allergic reaction *in vivo*. The representative pictures of hindpaw swelling, Evans blue exudation rate and hindpaw swelling rate of B-1023(A) and B-5023(B). (C) B-1023 and B-5023 inhibited C48/80-induced local skin mast cell degranulation in 10 μmol/L, scale bar = 50 μm; (D) The inhibition of B-1023 in body temperature decrease and serum histamine elevation induced by C48/80; (E) The inhibition of B-1023 in body temperature decrease serum histamine elevation induced by C48/80. Data are presented as mean ± SD ($n = 3$), ***$P < 0.001$, **$P < 0.01$ and *$P < 0.05$ *vs.* C48/80.

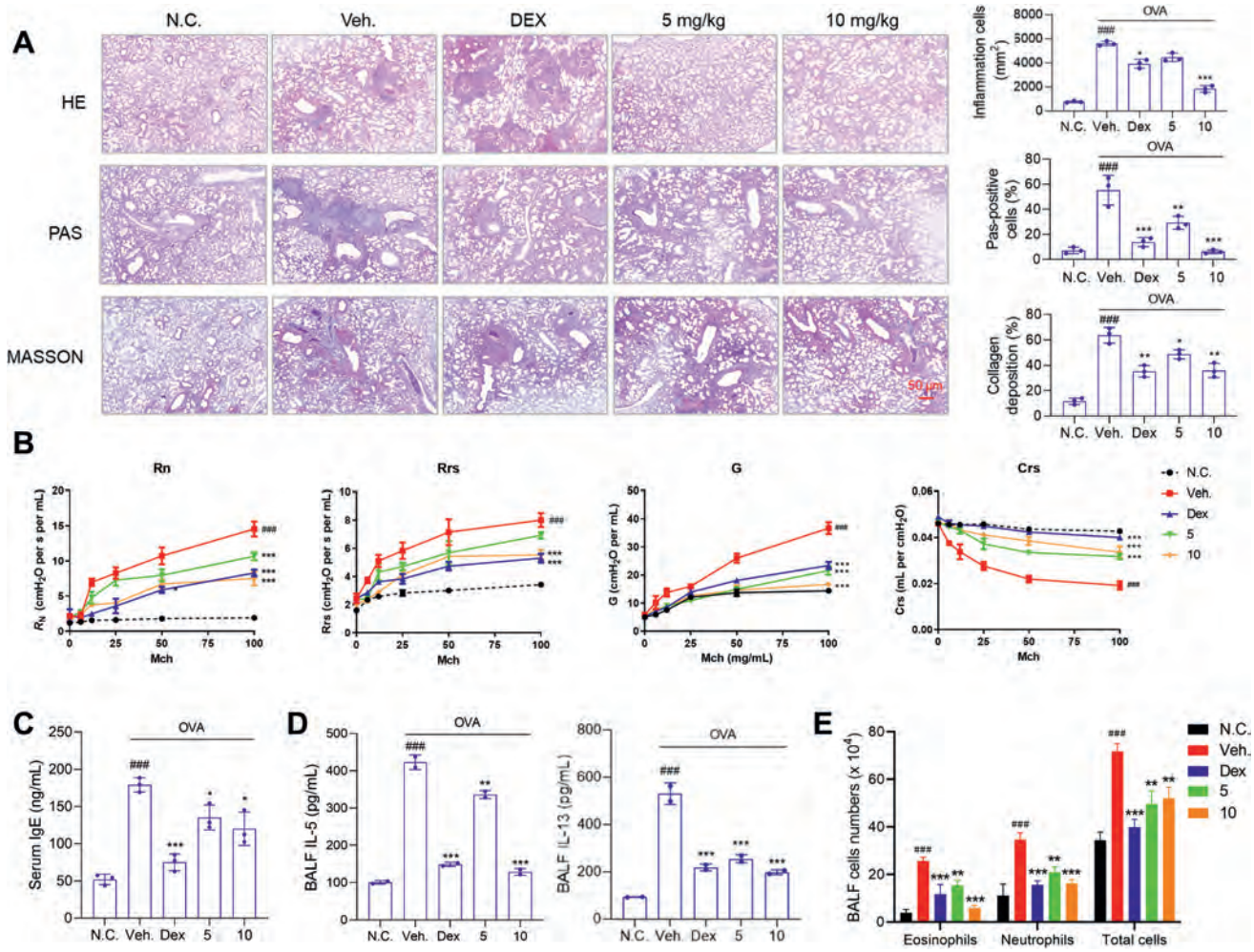

Figure 8 B-1023 effectively alleviated OVA induced AIPI. (A) Staining and statistics of lung tissue sections, data are presented as mean ± SD (n = 3), scale bar = 50 μm; (B) Airway hyperresponsiveness test; (C) Serum IgE concentration, data are presented as mean ± SD (n = 3); (D) cytokines concentration of BALF, data are presented as mean ± SD (n = 2); (E) The cell counts of eosinophil, neutrophil and total cells in BALF, $^{###}P < 0.001$ *vs.* N.C.; $^{***}P < 0.001$, $^{**}P < 0.01$ and $^{*}P < 0.05$ *vs.* Veh, data are presented as mean ± SD (n = 3).

as illustrated in Fig. 6A and B, and Supporting Information Fig. S3. The selectivity index (SI), which is a critical parameter representing the ratio of the cytotoxic concentration (CC_{50}) to the inhibitory concentration (IC_{50}), was found to be 689- and 129-fold for B-1023 and B-5023, respectively. This high SI value indicates that these compounds are safer and more effective. Therefore, to further evaluate the antiallergenic activities of B-1023 and B-5023, we investigated histamine release in LAD2 cells. As presented in Fig. 6C, both B-1023 and B-5023 inhibited the histamine release from LAD2 cells induced by C48/80 from 1 to 10 μmol/L. Additionally, when MRGPRX2 is chronically activated, cytokine are released. Therefore, the inhibitory effects of B-1023 and B-5023 on C48/80-induced interleukin-8 (IL-8) release in LAD2 cells were examined. As shown in Fig. 6D, both B-1023 and B-5023 reduced the IL-8 release induced by C48/80 at 1, 5, and 10 μmol/L. Overall, B-1023 and B-5023 exhibited resistance to mast cell degranulation induced by C48/80 *in vitro*, indicating that B-1023 and B-5023 are the most potent antiallergic precursors.

3.5. B-1023 and B-5023 alleviated C48/80-induced allergic reaction in vivo

We examined the inhibitory effects of B-1023 and B-5023 on local and systemic allergic reactions *in vivo*. The inhibitory effect on localized allergic reactions was assessed using hindpaw swelling assay (Fig. 7A and B). After intervention with B-1023 or B-5023, the swelling, and Evans blue exudation rates decreased in a dose-dependent manner at 1, 5, and 10 mg/kg. The toluidine blue staining of local skin (Fig. 7C) revealed that B-1023 and B-5023 reduced mast cell deformation and degranulation induced by C48/80. Both results suggested that B-1023 and B-5023 inhibited local allergic reactions induced by C48/80 *in vivo*. Regarding systemic allergic reactions, increased serum histamine will induce decreased body temperature. The body temperature change (Fig. 7D and E) showed that both compounds significantly attenuated the body temperature drop at 10 mg/kg induced by C48/80. Further, the serum histamine releases, when treated with B-1023 and B-5023, were reduced in a

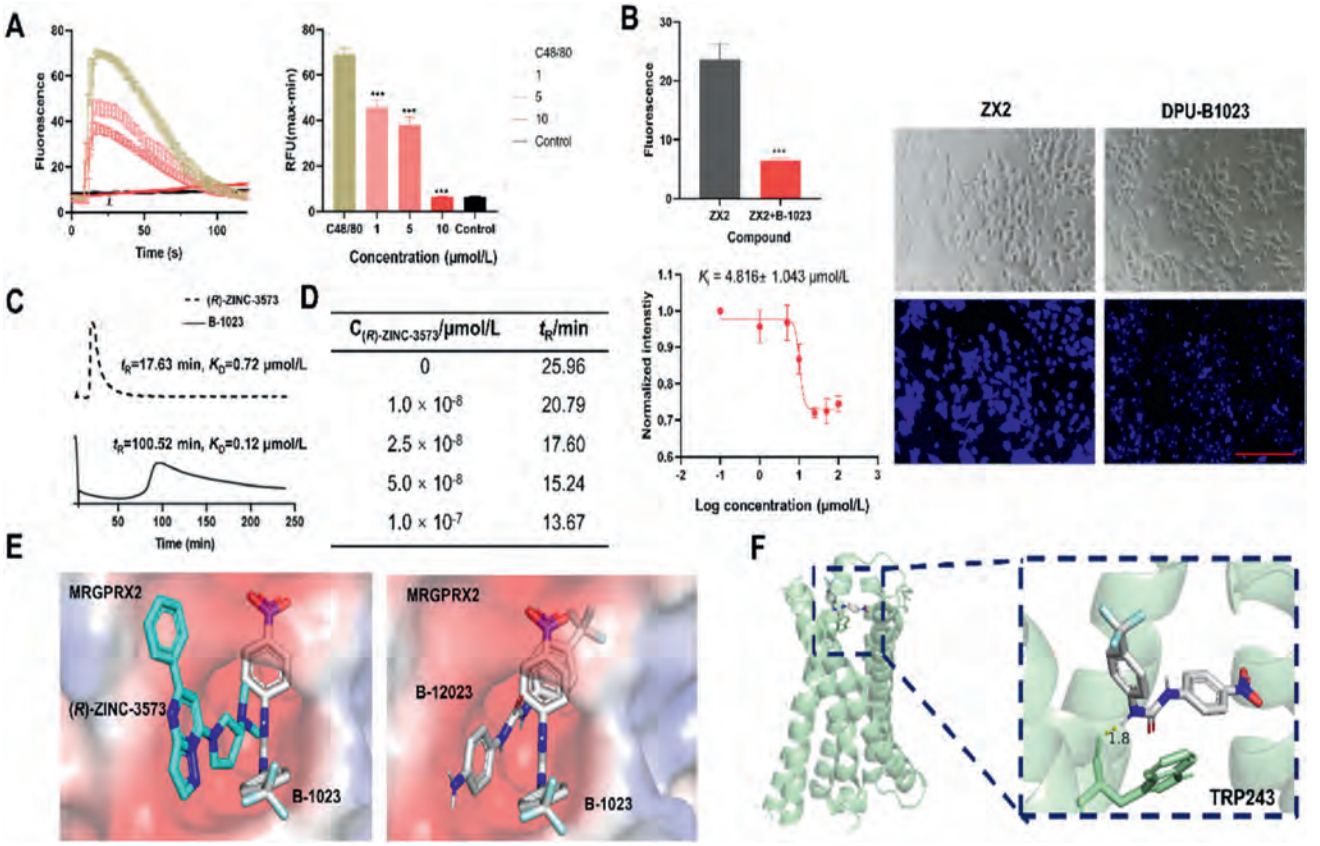

Figure 9 B-1023 competitively binds MRGPRX2. (A) B-1023 inhibited the calcium mobilization in MRGPRX2-HEK293 cells induced by 30 μg/mL C48/80; Data are presented as mean ± SD ($n = 3$), ***$P < 0.001$ *vs.* C48/80 group; (B) The fluorescence microscopy imaging, statistical diagram and K_i based on the competitive binding assay between B-1023 and ZX2, Scale bar = 50 μm; (C) The retention of B-1023 and (*R*)-ZINC-3573 on MRGPRX2-HEK293 cell membrane chromatography, and the K_D value was obtained by the relative standard method; (D) The summary of B-1023's retention time on the MRGPRX2-HEK293/CMC column with different concentrations of (*R*)-ZINC-2573; (E) Electrostatic potential energy molecular docking diagram of B-1023 and (*R*)-ZINC-3573 binding to MRGPRX2. (F) B-1023 binds to the TRP243 residue of MRGPRX2 with hydrogen bond.

dose-dependent manner at 1, 5, and 10 mg/kg, compared to that in the C48/80 group. Overall, B-1023 and B-5023 alleviated the C48/80-induced local and systemic allergic reactions in mice.

3.6. B-1023 effectively alleviated OVA-induced AIPI

Due to its antiallergic activity and safety, B-1023 was chosen for evaluation in the context of allergic disease animal modeling. AIPI is the ultimate manifestation of various allergic diseases, and based on this, we evaluated the effect of B-1023 in the context of AIPI. AIPI was induced in mice by OVA, as presented in Supporting Information Fig. S4. Dose of 5 or 10 mg/kg B-1023 were orally administered 30 min prior to each challenge. Staining of lung sections staining indicated obvious lesions in the Veh group. HE staining revealed significant inflammatory infiltration and airway thickening. PAS staining indicated the secretion of a large amount of mucus (glycogen), and MASSON staining revealed cord-like collagen deposition (Fig. 8A). Dexamethasone (Dex) improved lung lesions, and 5 mg/kg B-1023 exerted anti-AIPI effects, whereas 10 mg/kg B-1023 significantly attenuated the pathological changes, with a better effect than that of Dex (statistical bar chart on the right side of Fig. 8A). Meanwhile, AIPI mice exhibited obvious airway hyperresponsiveness (AHR), with increasing RN, Rrs, G and decreasing Crs, while B-1023 and Dex suppressed the AHR triggered by Mch (Fig. 8B). OVA-induced a significant increase in serum IgE levels in mice. Dex almost completely inhibited the excessive release of IgE, whereas 10 mg/kg B-1023 only partially weakened IgE release (Fig. 8C). However, Th2 cytokine (IL-5 and IL-13) release was obviously inhibited by B-1023 (Fig. 8D). Accordingly, the number of bronchoalveolar lavage fluid (BALF) cells was inhibited by B-1023 (Fig. 8E). The results demonstrated that B-1023 improved lung lesions and lung ventilation and reduced the release of IgE and cytokines, thus demonstrating the potential of B-1023 for treating allergic diseases, especially using as a therapy for treating allergic asthma. Given that B-1023 also mitigated the increase in serum histamine levels, we hypothesize that B-1023 may alleviate systemic allergic reactions, including but not limited to AIPI. Consequently, its therapeutic potential appears promising for other allergic conditions such as chronic urticaria and atopic dermatitis, warranting further investigation.

3.7. The correlation between B-1023 and MRGPRX2

To verify the interaction between the antagonists and MRGPRX2, we used B-1023 which exhibited slightly better activity as the research object, and evaluated the changes in intracellular calcium ion concentration and ligand-receptor binding characteristics. Intracellular Ca^{2+} acts as a second messenger after GPCR activation and is often

used as a judgment index to observe the effects of GPCRs[34]. Therefore, we tested the ability of B-1023 to inhibit calcium mobilization in MRGPRX2-HEK293 cells. The results are shown in Fig. 9A, B-1023 dose-dependently reduced C48/80-induced intracellular calcium mobilization at 1, 5, 10 μmol/L and this indicated that B-1023 is able to antagonize C48/80-induced MRGPRX2 activation. To further verify the binding site of B-1023 on MRGPRX2, we first performed a competition experiment using the fluorescent probe ZX2. ZX2 is a fluorescent probe designed by our team using the MRGPRX2 ligand (*R*)-ZINC-3573 as the recognition group[28]. The results of the competition experiment are presented in Fig. 9B. In the presence of B-1023, the fluorescence was lower, and this indicatied that B-1023 competed with ZX2 for the same combined site at a K_i of 4.816 ± 1.043 μmol/L. These results were also confirmed by cell membrane chromatography. The equilibrium dissociation constant (K_D) was determined using the relative standard method of cell membrane chromatography (Fig. 9C), and the K_D value of B-1023 was 0.12 μmol/L, which suggested that B-1023 possessed a certain binding affinity to MRGPRX2. When the concentration of (*R*)-ZINC-3573 in the mobile phase was 0, 1.0×10^{-8} mol/L, 2.5×10^{-8}, 5.0×10^{-8} and 1.0×10^{-7} mol/L, the retention times of B-1023 on the MRGPRX2-HEK293/CMC column were 25.96, 20.79, 17.60, 15.24 and 13.67 min, respectively (Fig. 9D and Supporting Information Fig. S5). The retention time of B-1023 decreased with increasing concentrations of (*R*)-ZINC-3573, indicating that B-1023 competitively bonded to (*R*)-ZINC-3573 at the same site. Furthermore, the molecular docking results demonstrated (Fig. 9E and F) that B-1023 bonds to the same cavity on MRGPRX2 as did (*R*)-ZINC-3573. A hydrogen bond was formed between the hydrogen atom of the urea group and TRP243 of the protein at a length of 1.8 Å, and this was a strong bond. B-1023 did not bind to GLU164 or ASP184, both of which are crucial for agonist recognition and activation. In summary, B-1023 competitively binds to MRGPRX2 and antagonizes the calcium mobilization induced by MRGPRX2 agonists, thereby exerting an antiallergic activity.

4. Conclusions

In the guidance of the "relative symmetry with electronegativity of different key-groups" strategy, 30 compounds were synthesized and evaluated. Finally, two most prominent compounds, B-1023 and B-5023, with relatively symmetric electron-withdrawing substituents and specific affinity for MRGPRX2, exhibited strong antiallergic activity at the submicromolar level *in vitro* and effectively alleviated AIPI *in vivo*. In conclusion, the development of B-1023 and B-5023 proved the feasibility and availability of the strategy, which could be new insight and reference to guide the design of other kinds of MRGPRX2 antagonists; on the other hand, the most priority compound, B-1023, will be further evaluated in certain MRGPRX2-related disease's models such as allergic asthma, hoping to provide a new treatment in the future.

Acknowledgments

This work was supported by the National Natural Science Foundation of China (grant Nos. 81930096 and 82373830).

Author contributions

Jiayu Lu: conceptualization, investigation and writing—original draft. Zhaomin Xia: conceptualization, methodology and writing—original draft. Yongjing Zhang: investigation, methodology and visualization, He Wang: investigation and visualization. Wen Yang: methodology and investigation. Siqi Wang: methodology and investigation. Nan Wang: supervision. Yun Liu: writing—review & editing and project administration. Huaizhen He: writing—review & editing, supervision and funding acquisition. Cheng Wang: writing—review & editing and supervision. Langchong He: conceptualization, rriting—review & editing and funding acquisition.

Conflicts of interest

The authors have no conflicts of interest to declare.

Appendix A. Supporting information

Supporting information to this article can be found online at https://doi.org/10.1016/j.apsb.2024.11.023.

References

1. Lang DM, Hsieh FH, Bernstein JA. Contemporary approaches to the diagnosis and management of physical urticaria. *Ann Allergy Asthma Immunol* 2013;**111**:235−41.
2. Leth Møller KB, Skaaby T, Linneberg A. Allergic rhinitis and allergic sensitisation are still increasing among Danish adults. *Allergy* 2020; **75**:660−8.
3. Wang XD, Zheng M, Lou HF, Wang CS, Zhang Y, Bo MY, et al. An increased prevalence of self-reported allergic rhinitis in major Chinese cities from 2005 to 2011. *Allergy* 2016;**71**:1170−80.
4. Laughter MR, Maymone MBC, Mashayekhi S, Arents BWM, Karimkhani C, Langan SM, et al. The global burden of atopic dermatitis: lessons from the Global Burden of Disease Study 1990−2017. *Br J Dermatol* 2021;**184**:304−9.
5. Wise SK, Damask C, Roland LT, Ebert C, Levy JM, Lin S, et al. International consensus statement on allergy and rhinology: allergic rhinitis−2023. *Int Forum Allergy Rhinol* 2023;**13**:293−859.
6. Eichenfield LF, Tom WL, Chamlin SL, Feldman SR, Hanifin JM, Simpson EL, et al. Guidelines of care for the management of atopic dermatitis: section 1. Diagnosis and assessment of atopic dermatitis. *J Am Acad Dermatol* 2014;**70**:338−51.
7. Mcneil BD, Pundir P, Meeker S, Han L, Undem BJ, Kulka M, et al. Identification of a mast-cell-specific receptor crucial for pseudo-allergic drug reactions. *Nature* 2015;**519**:237−41.
8. Baldo BA. MRGPRX2, drug pseudoallergies, inflammatory diseases, mechanisms and distinguishing MRGPRX2- and IgE/FcεRI-mediated events. *Br J Clin Pharmacol* 2023;**89**:3232−46.
9. Nattkemper LA, Tey HL, Valdes Rodriguez R, Lee H, Mollanazar NK, Albornoz C, et al. The genetics of chronic itch: gene expression in the skin of patients with atopic dermatitis andpsoriasis with severe itch. *J Invest Dermatol* 2018;**138**:1311−7.
10. Jia T, Che DL, Zheng Y, Zhang H, Li YX, Zhou T, et al. Mast cells initiate type 2 inflammation through tryptase released by MRGPRX2/MRGPRB2 activation in atopic dermatitis. *J Invest Dermatol* 2024;**144**:53−62.
11. Cao TBT, Cha HY, Yang EM, Ye YM. Elevated MRGPRX2 levels related to disease severity in patients with chronic spontaneous urticaria. *Allergy Asthma Immunol Res* 2021;**13**:498−506.
12. Plum T, Wang X, Rettel M, Krijgsveld J, Feyerabend TB, Rodewald HR. Human mast cell proteome reveals unique lineage, putative functions, and structural basis for cell ablation. *Immunity* 2020;**52**:404−16.
13. Ogasawara H, Noguchi M. Therapeutic potential of MRGPRX2 inhibitors on mast cells. *Cells* 2021;**10**:2906.
14. Wollam J, Solomon M, Villescaz C, Lanier M, Evans S, Bacon C, et al. Inhibition of mast cell degranulation by novel small molecule

MRGPRX2 antagonists. *J Allergy Clin Immunol* 2024;**154**: 1033−43.
15. Marion L, Marcus B, Liming H, Esther M, Marcos S, Brandon S, et al. Inventor; Escient pharmaceuticals Inc., assignee. Modulators of mas-related G-protein receptor X2 and related products and methods. Int patent US WO2022125636A1. 2022 Jun 16.
16. Wang J, Liu J, Yang Y, Sun G, Yang D, Yin SH, et al. Inhibitory effect of phellodendrine on C48/80-induced allergic reaction *in vitro* and *in vivo*. *Int Immunopharmacol* 2024;**134**:112256.
17. Wang N, Che DL, Zhang T, Liu R, Cao J, Wang J, et al. Saikosaponin A inhibits compound 48/80-induced pseudo-allergy *via* the Mrgprx2 pathway *in vitro* and *in vivo*. *Biochem Pharmacol* 2018; **148**:147−54.
18. Hou YJ, Che DL, Ma PY, Zhao TT, Zeng YN, Wang N. Anti-pseudo-allergy effect of isoliquiritigenin is MRGPRX2-dependent. *Immunol Lett* 2018;**198**:52−9.
19. Ding YY, Che DL, Li CM, Cao J, Wang J, Ma PY, et al. Quercetin inhibits Mrgprx2-induced pseudo-allergic reaction *via* PLCγ-IP3R related Ca^{2+} fluctuations. *Int Immunopharmacol* 2019;**66**:185−97.
20. Wang N, Wang J, Zhang YJ, Zeng YN, Hu SL, Bai HY, et al. Imperatorin ameliorates mast cell-mediated allergic airway inflammation by inhibiting MRGPRX2 and CamKII/ERK signaling pathway. *Biochem Pharmacol* 2021;**184**:114401.
21. Ogasawara H, Furuno M, Edamura K, Noguchi M. Novel MRGPRX2 antagonists inhibit IgE-independent activation of human umbilical cord blood-derived mast cells. *J Leukoc Biol* 2019;**106**:1069−77.
22. Bawazir M, Amponnawarat A, Hui Y, Oskeritzian CA, Ali H. Inhibition of MRGPRX2 but not FcεRI or MrgprB2-mediated mast cell degranulation by a small molecule inverse receptor agonist. *Front Immunol* 2022;**13**:1033794.
23. Kumar M, Duraisamy K, Annapureddy RR, Chan CB, Chow BKC. Novel small molecule MRGPRX2 antagonists inhibit a murine model of allergic reaction. *J Allergy Clin Immunol* 2023;**151**:1110−22.
24. Wong TK, Choi YG, Li PH, Chow BKC, Kumar M. MRGPRX2 antagonist GE1111 attenuated DNFB-induced atopic dermatitis in mice by reducing inflammatory cytokines and restoring skin integrity. *Front Immunol* 2024;**15**:1406438.
25. Wang C, Hu T, Lu JY, Lv YX, Ge S, Hou YJ, et al. Convenient diaryl ureas as promising anti-pseudo-allergic agents. *J Med Chem* 2022;**65**: 10626−37.
26. Han SL, Lv YN, Kong LY, Che DL, Liu R, Fu J, et al. Use of the relative release index for histamine in LAD2 cells to evaluate the potential anaphylactoid effects of drugs. *Sci Rep* 2017;**7**:13714.
27. Ma WN, Yang L, Lv YN, Fu J, Zhang YM, He LC. Determine equilibrium dissociation constant of drug-membrane receptor affinity using the cell membrane chromatography relative standard method. *J Chromatogr A* 2017;**1503**:12−20.
28. Hou YJ, Wang C, Lu JY, Jia M, Lv YX, Jia X, et al. Design and synthesis of first environment-sensitive coumarin fluorescent agonists for MrgX2. *Int J Biol Macromol* 2022;**203**:481−91.
29. Ma WN, Zhang DD, Li J, Che DL, Liu R, Zhang J, et al. Interactions between histamine H1 receptor and its antagonists by using cell membrane chromatography method. *J Pharm Pharmacol* 2015;**67**: 1567−74.
30. Jiang CY, Han S, Chen TG, Chen JZ. 3D-QSAR and docking studies of arylmethylamine-based DPP IV inhibitors. *Acta Pharm Sin B* 2012; **2**:411−20.
31. Marshall CM, Federice JG, Bell CN, Cox PB, Njardarson JT. An update on the nitrogen heterocycle compositions and properties of U.S. FDA-Approved pharmaceuticals (2013−2023). *J Med Chem* 2024;**67**:11622−55.
32. Hermans MAW, Van Stigt AC, Van De Meerendonk S, Schrijver B, Van Daele PLA, Van Hagen PM, et al. Human mast cell Line HMC1 expresses functional Mas-related G-protein coupled receptor 2. *Front Immunol* 2021;**12**:625284.
33. Cao C, Kang HJ, Singh I, Chen H, Zhang C, Ye W, et al. Structure, function and pharmacology of human itch GPCRs. *Nature* 2021;**600**:170−5.
34. Berridge MJ, Bootman MD, Roderick HL. Calcium signalling: dynamics, homeostasis and remodelling. *Nat Rev Mol Cell Biol* 2003;**4**: 517−29.